Failure mechanism of concrete under biaxial fatigue load

Bin Mu & S. P. Shah

Center for ACBM, Northwestern University, Evanston, IL 60208, U.S.A.

ABSTRACT: The paper is focusing on the fatigue response of concrete subjected to biaxial stresses in the compressive-compression-tension (c-C-T) region. where the principal tensile stress is smaller in magnitude than the principal compressive stress. Crack information including crack formation and propagation under controlled conditions for static and fatigue loading was studied. The crack propagation will be modeled using the principles of fracture mechanics.

Keywords: Fatigue, fracture, failure, biaxial load, concrete

1 INTRODUCTION

Low frequency and high–amplitude cyclic loads that are applied on a concrete airport pavement slab are especially critical to the fatigue response of concrete pavement. According to classical theory, such loads result in in-plane tensile stresses at the bottom of the top layer of the pavement structures. In an actual pavement slab, the reaction of the underlying subgrade to the applied wheel load results in a compressive stress component at the bottom of the slab, which is normal to the in-plane tensile stress. Thus, the critical stress field in concrete pavements, when considering the fatigue behavior is a triaxial combination of tensile and compressive stresses. This triaxial stress field can be simplified to biaxial tensile and compressive stress field by neglecting one of the horizontal (in-plane) tensile stresses. The different signs of the principle stresses form a biaxial Compression-Tension stress region (C-T region). The C-T region can be further divided into two sub-regions. One is called t-C-T sub-region, where the principle tensile stress is larger than, in magnitude, the principle compressive stress, and the other is called c-C-T region, where the principle tensile stress is smaller than, in magnitude, the principle compressive stress (Fig.1).

An investigation to characterize the static and low-cycle fatigue response of airport concrete pavement subjected to biaxial stresses in the t-C-T region was performed at the NSF Center of Advanced Cement Based Materials (ACBM) of the Northwestern University. The experimental setup consisted of the following test configurations: (a) notched concrete beams tested in three-point bend configuration, and (b) hollow concrete cylinders subjected to torsion with or without superimposed axial tensile force (Fig.1). The damage imparted to the material was examined using mechanical measurements and an independent nondestructive evaluation (NDE) technique based on vibration measurements. The failure of concrete in t-C-T region under static and fatigue loading was governed by a single crack propagation. A fracture-based fatigue failure criterion was proposed, wherein the fatigue failure can be predicted using the critical mode I stress intensity factor (SIF). The crack growth rate followed a two-stage trend: a deceleration stage, which was governed by the R-curve of the specimen, and an acceleration stage, which was governed by the Paris law. Details of the experimental work and the analytical model for the material response are available in the References (Subramaniam *et al.* 1998, Subramaniam 1999a, Subramaniam *et. al.* 1999b, Subramaniam *et al.* 2000, Subramaniam *et al.* 2002). The current investigation focused on the fatigue behavior of concrete subjected to the biaxial c-C-T region. It was proposed to extend previous experimental/analytical methods and results from t-C-T region to the biaxial loading in

the c-C-T region. The typical loading case of point-V was investigated. The experimental details for concrete cylinders under compression (point-IV) were shown the References (Mu, *et. al.* 2003).
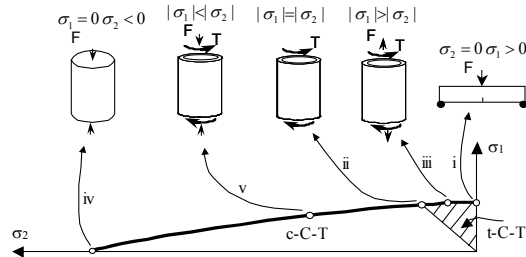

Figure 1. The biaxial C-T region

2 EXPERIMENTAL DETAILS

Concrete hollow cylinders were 101.6 mm in outer diameter, 57.15 mm in inner diameter, and 203.2 mm in length. The mixture proportion is: cement: water: coarse aggregate: fine aggregate = 1.0:0.5:2.0:2.0 (by weight). The ends of the hollow cylinders were reinforced with 12.7 mm x 12.7 mm steel wire mesh cages that were embedded into the concrete to ensure that failure happens in the gage section away from the ends. The mesh extended a length of 63.5 mm from both ends and was continuous in the circumferential direction (Fig.2). The mesh cage had a diameter of approximately 91.4 mm. The average age of specimens used for the test was over 6 months to ensure mature concrete.
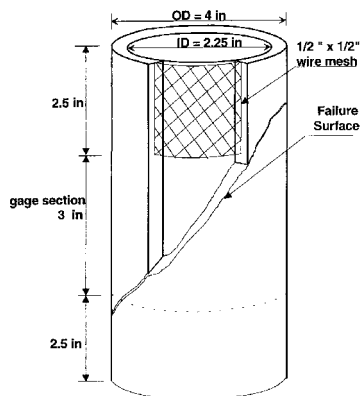

Figure 2. Specimen

During the test, the ratio of compression and torsion was kept constant so as to keep the ratio of the two principal stresses remained constant as 1.5 throughout the loading process, i.e. proportional loading was used.

Instrumentation was shown in Fig.3. Four equally spaced LVDTs along the circumference were used to measure the relative axial displacement. The relative rotation of the two rings was measured by two LVDTs mounted on one ring in the horizontal direction (tangential to the ring) and the measured change in length was converted to the change of angle between the two rings. The axial LVDTs have a range of ±0.5 mm and rotational LVDTs have a range of ±0.25 mm. The specimen was connected to the MTS by two steel caps.

Figure 3. Experimental setup: LVDTs

To limit test instability and therefore have stable control in specimens that exhibit snapback behavior, a measurable test parameter, which increases monotonically throughout the destruction of the specimen is needed. In this way, using a failure sensitive parameter as the feedback signal can eliminate the test instability. Therefore a test parameter, which monitors the response of the failure zone would be an appropriate feedback signal to control snapback. Okubo and Nishimatsu (1985) proposed a control method in which a linear combination of load and displacement is used as the feedback signal in a closed loop servo controlled test machine. In this study of concrete hollow cylinders subjected to combined compression and torsion, the feedback signal, which was a linear combination of gage rotation and torque was used to obtain the complete torque-gage rotation curves. It has the form

$$Feedback\ Signal = \theta - \alpha \frac{T}{K_0} \qquad (1)$$

where K_0 is the initial tangent modulus of the torque-gage rotation curve and is found to be

around 46,000 N-m/deg. T and θ are the applied torque and the rotation of the gage section, respectively. α is a coefficient, which is found to be around 0.8 for a stable control.

In the static test, a rate of 2.0×10^{-5} deg/sec was used for Eq.(1). In Fatigue test, three different torque ranges were conducted. Torque was applied between two fixed torque levels in a sinusoidal waveform at a frequency of 2 Hz. The tests were performed in a torque control. The lower limit of the torque was kept as 5% of the average static peak torque value. Three different upper limits were used corresponding to 90%, 85% and 80% of the average static peak torque.

3 EXPERIMENTAL RESULTS

3.1 *Static combined compression and torsion*

A typical torque vs. gage rotation curve for tests under combined compression and torsion is shown in Fig.4. The torque and gage rotation values have been normalized with respect to peak torque and the gage rotation corresponding to the peak torque, respectively. During the test, the samples were unloaded and reloaded in the post-peak period at around 90%, 80% and 70% of the peak strength, respectively to obtain the compliance of the specimen in the post peak period. Closed-loop testing manner was used with a combined signal given by Eq.(1) till the first unloading started at 90% of the peak strength in the post-peak period. At the first unloading process at 90% of the peak strength, the control mode was shifted to the rotation gage for the rest of the testing region. The percentage increase in rotational compliance is calculated with respect to the initial rotational compliance (the most linear part of the pre-peak torque-gage rotation curve). The rotational compliance corresponding to each unloading-reloading loop represents secant compliance calculated between the top and the bottom intersection points of the unloading-reloading curves. The increase in rotational compliance in the post-peak part can be attributed to the propagation of cracking in the gage region as shown below.

Fig.5 shows the extension of the four axial LVDTs with respect to normalized test time. The crack growth can be traced by the variation of the axial LVDTs. It can be seen that LVDT 2 & 3 increased while LVDT 1 & 4 decreased after the peak load (normalized time = 1.0). The difference of the extensions of the four axial LVDTs after the peak load apparently indicated a bending effect. This bending effect was produced by the initiation and propagation of an inclined crack as observed in

the experiment. This crack formed between LVDT 2 & 3. In the experiment, it was found that the crack was inclined at an angle around 51° with respect to the horizontal (Fig.6).
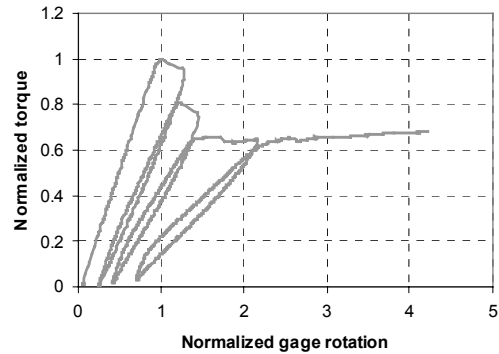

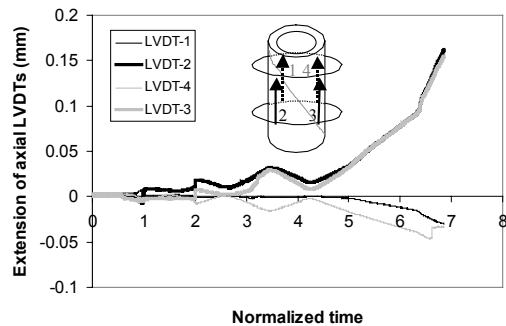Figure. 4 Torque vs. gage rotation for static test

Figure 5. Extension of the four axial LVDTs

Figure 6. An inclined crack in the hollow cylinder specimens

Corelating Fig.4 and Fig.5, it can be seen that the average axial deformation is closely related to the increase in the rotational compliance of the specimen. This increase in the rotational

compliance of the specimen can be attributed to the propagation of a crack in the gage region.

3.2 Fatigue combined compression and torsion

A typical fatigue response of a specimen is shown in Fig.7. There is a steady increase in the rotational compliance as seen by the decrease slope of the loading-unloading curves. The axial displacements measured by the four axial LVDTs mounted on the same specimen during the fatigue test are shown in Fig.8. The trends in axial displacement correspond well with the observed change in rotation compliance. This suggests a possible connection between the two phenomena. LVDT-3 shows an increase in axial displacement while LVDT-1 shows a decrease in the measured axial displacement. In the experiment, it was observed that an inclined crack initiated and propagated between LVDT-2, 3 & 4 (Fig.8). From the static response, it has been established that the different extensions of axial LVDTs correspond to crack propagation in the gage section. Thus, formation and propagation of a crack in the gage section appears to be the mechanism of failure for the fatigue loading.
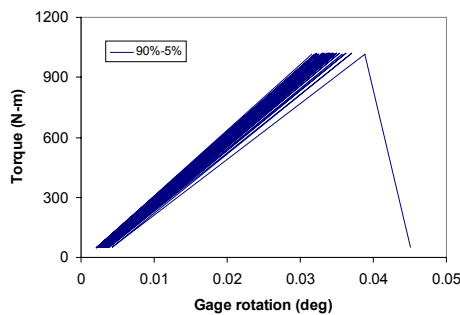
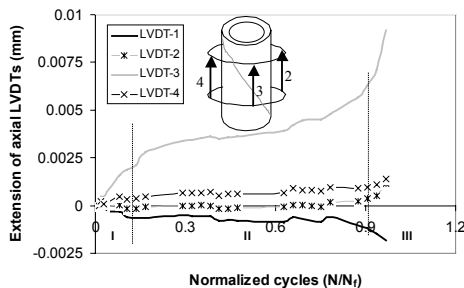Figure. 7 A typical fatigue response of a specimen

Figure. 8 Extensions of axial LVDTs during the fatigue test

The extensions of axial LVDTs suggest that the damage localized into a single crack in the first few cycles of loading (stage I). The crack propagates at a steady rate in the subsequent cycles (stage II). Failure occurs when the crack grows to a size that cannot be safely supported by the applied load (stage III).

4 MODEL FOR FATIGUE FAILURE OF CONCRETE UNDER COMPRESSION AND TORSION

From the experiment of concrete under combined compression and torsion, it can be seen that as a general loading point in the biaxial c-C-T region (point-V in Fig.1), where the principle compressive stress is 50% larger than the principle tensile stress, both the static failure and fatigue failure are due to the propagation of a single localized inclined crack. Experimental evidence suggests that the increase in rotational compliance during the compressive and torsional test is a result of this crack growth. To model fatigue failure, it is assumed that the response is due to growth of a single crack. The length of this crack was calculated from the compliance measurement and using linear elastic fracture mechanics. A comparison of rotational compliance at ultimate failure in fatigue and at different points in the post-peak part of the static response is shown in Fig.9. The normalized rotational compliance in fatigue was calculated with respect to the rotational compliance in the first cycle. It can be found that the static response is comparable to the fatigue response.
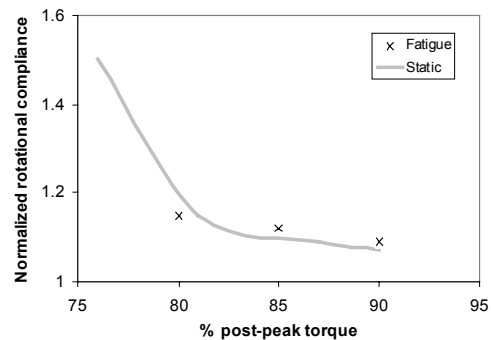
Figure. 9 A comparison of static and fatigue response: Torque – compliance

Direct measurement of crack length is difficult in the concrete hollow cylinders. The relationship between the crack length and rotational compliance of the specimen can be established by numerical

method (FEM) using the principles of LEFM. Detailed FEM simulation for concrete hollow cylinders under pure torsion was carried out by Subramaniam (1999a). He discussed the crack front profiles, stress intensity factors (K_I, K_{II}, K_{III}), and crack propagation criterion, and found that the crack growth of concrete hollow cylinder under the pure torsion was due to the principle tensile stress and was governed by the critical Mode I SIF, K_{IC}.

$$K_I = K_{IC} \qquad (2)$$

Using FEM, he presented the relationship between the Mode I SIF, K_I, crack length, a, and applied torque as:

$$K_I = (2.6 \times 10^{-6}(a) + 7.2 \times 10^{-6}) * \text{Torque} \qquad (3)$$

where K_I is in $\text{N/mm}^{3/2}$, Torque is in N-mm, and a is in mm.

Eq.(3) was obtained from the pure torsional case. At this loading case, if assuming a linear shear stress distribution along the thickness direction, the crack surface is planar along the thickness direction. By calculation, it was found that even under the combined compressive & torsional loading case, the crack surface is still close to a plane as observed in the case of pure torsional loading.

Since the failure of hollow specimens under the combined compression & torsion is quite similar to that under the pure torsion (both due to the crack propagation by the principle tensile stress), it is reasonable to extend the relationship of Eq.(3) to the combined compressive & torsional loading case. However, due to a change of direction and magnitude of the principle tensile stress, the applied torque, which generates the principle tensile stress, should be modified by multiplying a factor.

$$K_I = (2.6 \times 10^{-6}(a) + 7.2 \times 10^{-6}) * \sqrt{-c} * \text{Torque} \qquad (3a)$$

where K_I is in $\text{N/mm}^{3/2}$, Torque is in N-mm, and a is in mm. c is the ratio of the principle tensile stress to the compressive stress.

In the previous research on the t-C-T region, it has been shown that both static and fatigue failure were due to the Mode I crack propagation and governed by the critical Mode I SIF, K_{IC}. For this mix proportion, $K_{IC} = 38 \ \text{N/mm}^{3/2}$. Under combined compression and torsion, the failure was observed very similar to those in the t-C-T region (due to the crack propagation). Thus, it is assumed that under static combined compression and torsion the post-peak torque vs. rotation curve was also governed by the Mode I SIF, K_{IC}. The crack length at any point in post-peak part of the static response can be calculated from the increase in unloading/reloading compliance from the following equation:

Torsional compliance =
$$5.2 \times 10^{-3} * (a)^2 - 7.1 \times 10^{-2} * (a) + 1.0 \qquad (5)$$

where a is in mm.

The rate of fatigue crack growth ($\Delta a / \Delta N$) for the same specimen is shown in Fig.10. It can be seen that the crack growth also follows a two-stage process: a deceleration stage followed by an acceleration stage up to failure. There is an inflection point (minimum) corresponding to a critical crack length, $a_{critical}$, where the rate of crack growth changes from deceleration to acceleration. This critical crack length is found to be around 11.2 mm from Fig.10. On the other hand, from Eq.(3) it can be calculated that the crack length corresponding to the static peak load, a_{peak}, is around 12.2 mm. Then $a_{critical} \approx a_{peak}$. This means that under the term of crack length, the inflection point in fatigue test corresponds to the peak point in the static test. The deceleration stage typically lasts for around the first forty five percent of the fatigue life of the specimens.
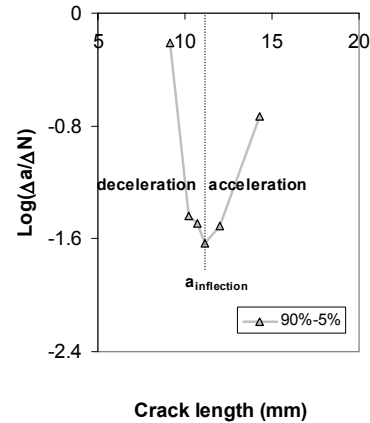

Figure 10. Crack growth during fatigue test

A comparison of crack length at fatigue failure to those at different unloading/reloading points in the static post-peak period is shown in Fig.11. It can be seen that the crack lengths at fatigue failure compare favorably with the crack lengths at the corresponding load in the static post-peak response of the specimen. This suggests that the crack length at fatigue failure can be obtained from the static response. Hence the static response acts as a failure-envelope to the fatigue response if framed in term of crack length. Further more, Eq.(3) ($K_I = K_{IC}$) represents the failure criterion for the fatigue loading.
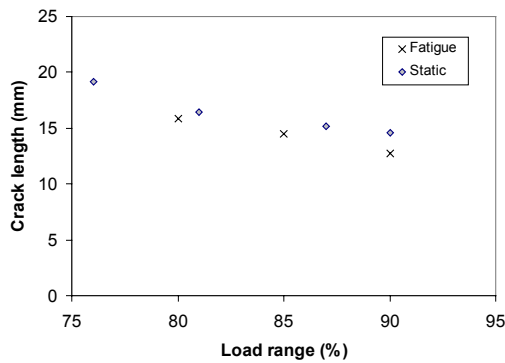
Figure 11. A comparison of static and fatigue response:
Torque – crack length

From the previous research in t-C-T region, it is proposed that the crack growth rate at the deceleration stage is governed by the increasing resistance (R curve), and it is governed by the Mode I SIF (Paris law) in the acceleration stage. In the deceleration stage, the crack growth rate can be expressed as

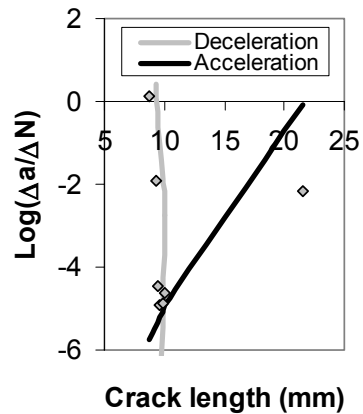$$Log\,(\Delta a\,/\,\Delta N) = Log\,(C_1) + n_1 Log\,(a - a_0) \quad (6a)$$

In acceleration stage, the crack growth rate can be expressed as

$$Log(\Delta a\,/\,\Delta N) = Log(C_2) + n_2 Log(\Delta K_I) \quad (6b)$$

Where a_0 is the initial crack length (assumed to be 2 mm). $Log(C_1)$, n_1, $Log(C_2)$ and n_2 are constants. The units of crack length, a, and K_I, are mm and N/mm$^{3/2}$, respectively.
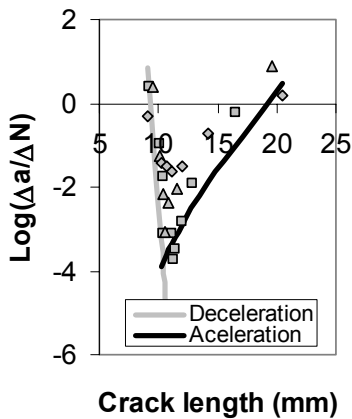

(a)
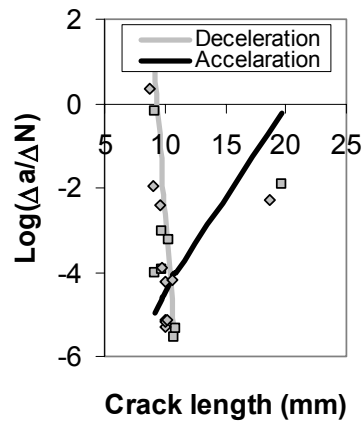
(b)

(c)

Figure 12. A comparison between analytical prediction and experiment: (a) 90%-5% (b) 85%-5% and (c) 80%-5%

A comparison of the experimental data from the combined compressive & torsioal tests and the model predictions from the deceleration and acceleration stages is shown in Fig.12. In the deceleration stage (Eq.6a), the value of $Log(C_1)$ and n_1 were taken to be 59.6 and –68.8, respectively. The Paris law constants (Eq.6b), $Log(C_2)$ and n_2, were taken to be –28.6 and 17.33, respectively, same as the average value of the previous research in the t-C-T region calibrated from the flexural test. It can be seen that there is a reasonable match between the experimental data and model predictions. So the previously proposed model can be successfully extended to concrete

subjected to combined compression and torsion in the c-C-T region. However, the parameters in the deceleration stage are different from those calibrated from the flexural response of concrete. The fatigue crack rate growth at the acceleration stage can be predicted using the uniaxial material parameters.

5 CONCLUSIONS

The objective of this work is to characterize the static and fatigue response of concrete subjected to combined compression and torsion in the compression region (c-C-T region), where the principle compressive stress is larger in magnitude than the principle tensile stress. It is proposed to extend/verified the previous methods and results in the biaxial tension region (t-C-T region) to/in the biaxial compression region (c-C-T region).

Hollow concrete cylinders subjected to combined compression and torsion were used to represent the biaxial loading in the compression region. The instability around the peak load in the static test was prevented by using the combined signal controlling method. The previously proposed models in the t-C-T region were verified by the new experimental data in the c-C-T region.
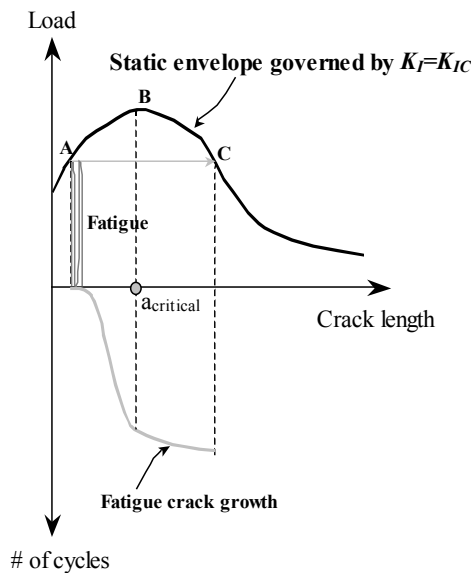

Figure 13 Schematic representation of crack growth in static and fatigue loading

In the investigation, the static load response can be visualized as a failure envelope curve in c-C-T region, where each point in the post-peak region is an equilibrium point representing the maximum load that can be supported for a given level of damage. Therefore every point on the post-peak load envelope can be characterized by a given damage level. Further, it can be implicitly assumed that the change in stiffness/compliance of a specimen is due to accruing damage in the specimen and the decrease/increase in stiffness/compliance is indicative of the increase in level of damage.

The crack growth in the static and fatigue loading can be schematically represented by Fig.13. In the figure, the fatigue response of concrete is from A to C. At failure point, C, the crack length is comparable with that of the static response. The crack growth rate is decelerated from A to B and is accelerated from B to C. The critical crack length, $a_{critical}$, corresponds to the peak load of the static response.

6 ACKNOWLEDGEMENT

7 REFERENCES

Mu, B., Subramaniam, K. V. & Shah, S. P. 2003. Failure Mechanism of Concrete under Fatigue Compressive Load. Journal of Materials in Civil Engineering, accepted (MT/2003/022651).

Okubo, S. & Nishimatsu, Y. 1985. Uniaxial Compression Testing Using a Linear Combination of Stress and Strain as the Control Variable. International Journal of Rock Mech. Min. Sci. & Geomech. Abstr 22(5): 323-330.

Subramaniam, K. V., Popovics, J.S., & Shah, S. P. 2002. Fatigue Fracture of Concrete Subjected to Biaxial Stresses

in the Tensile *C–T* Region. Journal of Engineering Mechanics, ASCE 128(6): 668-676.

Subramaniam, K. V., O'Neil, E., Popovics, J.S. & Shah, S.P. 2000. Flexural Fatigue of Concrete: Experiments and Theoretical Model. Journal of Engineering Mechanics, ASCE 126(9): 891-898.

Subramaniam, K. V. (1999a). Fatigue of Concrete Subjected to Biaxial Loading in the Tension Region. *PhD dissertation*, Northwestern University, Evanston, IL.

Subramaniam, K. V., Popovics, J.S. & Shah, S.P. 1999b. Fatigue Behavior of Concrete subjected to Biaxial Stresses in the C-T Region. ACI Materials Journal 96(6): 663-669.

Subramaniam, K. V., Popovics, J.S. & Shah, S.P. 1998. Testing Concrete in Torsion: Instability Analysis and Experiments. Journal of Engineering Mechanics, ASCE, 124(11): 1258-1268.